

# The one body density matrix of a quantum bright soliton from the coordinate Bethe ansatz

Alex Ayet<sup>1,2</sup> and Joachim Brand<sup>1</sup>

<sup>1</sup>*Dodd-Walls Centre for Photonics and Quantum Technologies, Centre for Theoretical Chemistry and Physics, and New Zealand Institute for Advanced Study, Massey University, Private Bag 102904, North Shore, Auckland 0745, New Zealand*

<sup>2</sup>*Ecole Normale Supérieure, 45 rue d'Ulm, 75005 Paris, France*

We present a novel approach for computing reduced density matrices for superpositions of eigenstates of a Bethe-ansatz solvable model by direct integration of the wave function in coordinate representation. A diagrammatic approach is developed to keep track of relevant terms and identify symmetries, which helps to reduce the number of terms that have to be evaluated numerically. As a first application we compute with modest numerical resources the one-body density matrix and its eigenvalues including the condensate fraction for a quantum bright soliton with  $N = 10$  bosons. The latter are constructed as superpositions of string-type Bethe-ansatz eigenstates of nonrelativistic bosons in one spatial dimension with attractive contact interaction. Upon delocalising the superposition in momentum space we find that the condensate fraction saturates to a value close to one. The presented approach is suitable for studying time-dependent problems and generalises to higher-order correlation functions.

## I. INTRODUCTION

The study of one dimensional interacting bosons is an exciting field of ultra cold atomic physics where experimental results can match the theoretical predictions with an impressive precision<sup>1–3</sup>. In the past few years, quasi-one-dimensional atomic gases have been realized experimentally<sup>4–6</sup>, with the possibility to tune the interaction strength between particles, allowing comparison with theory.

The Lieb-Liniger model used to describe point-like bosons in one dimension interacting via contact interactions is exactly solvable using the Bethe ansatz<sup>7</sup>. A wider class of Bethe-ansatz solvable models like the Heisenberg spin chain and the Hubbard model at half filling share a closely related mathematical structure of eigenfunctions<sup>8</sup>. Even though the Bethe ansatz provides the eigenfunctions of a given model Hamiltonian in explicit form, it is still very difficult to evaluate many quantities of interest including general correlation functions. The introduction of the inverse quantum scattering method and its evolution into the algebraic Bethe ansatz<sup>9</sup>, has enabled significant progress. In particular the norm of the eigenstates<sup>10</sup> and certain one- and two-particle correlation functions of the ground state<sup>11</sup> could be computed.

The coordinate Bethe ansatz refers to the original formulation of the Lieb-Liniger model, where the eigenstates were provided in coordinate representation<sup>7</sup>. Although any correlation function can be expressed by integrals over the eigenstates, the exponentially large number of terms often proves prohibitive beyond a very small number of particles. Only in very specific cases could closed form expressions for correlation functions be found. Examples for bound states of attractively interacting bosons are the particle density under the condition of a fixed center of mass position<sup>12,13</sup> and the particle density of a superposition of bound states<sup>14</sup>. In this paper we compute

the full single-particle density matrix of a superposition of bound states, which requires more general form factors than computed previously, in Ref. [14] or by means of the algebraic Bethe ansatz in Ref. [11]. We note that the coordinate Bethe ansatz has recently been used to calculate correlation functions for the repulsively interacting Bose gas in Ref. [15].

In comparison with the 1D Bose gas with repulsive interactions, much less attention has been paid to attractive interactions. Experimental realisations with ultra-cold atoms<sup>16–20</sup> have mostly been interpreted in terms of the Gross-Pitaevskii mean field theory, which leads to a cubic nonlinear Schrödinger equation, while some theoretical works<sup>21–23</sup> highlight the interesting physics that remains to be studied. The particularity of this regime is that the eigenstates of the system are correlated bound states<sup>24</sup> that behave like a particle. Although these states are delocalized in space, a localized state can be constructed by a proper superposition. These are quantum bright solitons, which exhibit a peak in their density, and have been studied in the past<sup>14</sup>, even though only their density profile has been computed. They differ from the classical soliton solutions of the non-linear Schrödinger equation<sup>25</sup> in their time evolution. Indeed, the center of mass of a quantum soliton will spread over time in order to recover the translational invariance of the system. Unlike the classical soliton, it does not conserve its shape over time. Other features are yet to be studied, as their collision and their high-order correlation functions. This study is of special interest as bright solitons in Bose-Einstein condensates have been realized experimentally<sup>16,20</sup>, and understanding the features that the Gross-Pitaevskii approximation is missing is thus of special importance.

In this article we present a method to compute the full one-body density matrix of such a solitonic state, using a similar starting point to the one in Ref. [14]. While closed form expressions can be easily derived for the diagonal elements, the complexity of the integrals that need to

be computed for the off diagonal elements requires a numerical implementation. We introduce a diagrammatic representation of these that simplifies the manipulation and allows for a very efficient computation of the relevant form factors. On the one hand the approach yields new results such as the full density matrix and its time evolution, which gives access, via diagonalization, to the condensed fraction of the quantum bright soliton. On the other hand it is a method that can be easily generalised to provide access to higher order correlation functions or for the study of more complex dynamics.

The paper is organized as follows. We recapitulate the coordinate Bethe Ansatz formalism and the form of the eigenstates of the system in the attractive case in Section II, followed by a discussion on the solitonic state we are studying in Section III. After explaining the approach for the calculating the density matrix in Sections IV and V, we discuss numerical results in Section VI.

## II. THE COORDINATE BETHE ANSATZ FORMALISM

The Lieb-Liniger model represents a one dimensional system of  $N$  bosons interacting with a contact potential of strength  $c$ . For  $x_i$  the coordinates of the particles, the Hamiltonian of the model is

$$H = - \sum_{i=1}^N \frac{\partial^2}{\partial x_i^2} + 2c \sum_{\langle i,j \rangle} \delta(x_i - x_j), \quad (1)$$

where the sum is over all the pairs of particles.

The coordinate Bethe Ansatz gives an explicit form for the eigenstates of the Schrödinger equation associated with the Hamiltonian (1), in the position representation. If we denote by  $2L$  the size of the system, we can write them in the *fundamental domain*  $-L \leq x_1 \leq x_2 \leq \dots \leq x_N \leq L$  in the form

$$\langle \{x_i\} | \{k_i\} \rangle = \sum_{\mathcal{P} \in S(N)} a(\mathcal{P}) e^{\sum_i k_{\mathcal{P}(i)} x_i}, \quad (2)$$

where  $S(N)$  is the set of all permutations on  $1, \dots, N$  and the  $k_i$  are called *quasi-momenta*. They can be either real or complex, depending on sign of  $c$ . The wave function on the whole domain can be reconstructed by bosonic symmetry.

The contact potential in Eq. (1) imposes boundary conditions for  $x_i = x_j$ , and leads to constraints over the coefficients  $a(\mathcal{P})$  that have to satisfy the following set of equations:

$$a(\mathcal{P}') = \frac{k_{\mathcal{P}(i+1)} - k_{\mathcal{P}(i)} + ic}{k_{\mathcal{P}(i+1)} - k_{\mathcal{P}(i)} - ic} a(\mathcal{P}), \quad (3)$$

where  $\mathcal{P}'$  is derived from  $\mathcal{P}$  by exchanging the  $i$ -th and the  $(i+1)$ -th component of the permutation.

In the following, we are interested in the attractive case characterized by  $c$  being negative, in which the eigenstates of the system are the so called string states. In the regime of a large  $L$  and finite  $N$ , their quasi-momenta are complex, and form strings along the imaginary axis. The ground state and the first excited states, denoted by  $|p\rangle$ , are made of one string centered on the real axis on a value  $p$ , and the quasi-momenta of the particles are then

$$k_j = p + i \frac{c}{2} (N - 2j + 1) + \delta_j \quad j \in \{1, \dots, N\}, \quad (4)$$

with  $\delta_j \sim e^{-(cst)L}$  called the string deviations. In the following, we will neglect them, which becomes exact in the limit of large box size  $2L$ .

The string states are eigenstates of the momentum operator of the whole system with eigenvalues  $Np$ , the total momentum of the string. It follows from Eq. (3) that all the coefficients  $a(\mathcal{P})$  vanish except for the identity permutation, when using the string quasi-momenta of Eq. (4).

The final wave function, *valid outside of the fundamental domain*, for a simple string state (4), is thus

$$\langle \{x_i\} | p \rangle = \mathcal{N} e^{ip \sum_{j=1}^N x_j + \frac{c}{2} \sum_{1 \leq i \leq j \leq N} |x_j - x_i|}. \quad (5)$$

We see that these are bound states, as they are exponentially localized in the distance between the particles. They are eigenstates of the Hamiltonian (1) with energy

$$E_p = Np^2 - \frac{c^2}{12} N(N^2 - 1). \quad (6)$$

We end this section by giving the normalization factor of the eigenstates for our numerical setup

$$\mathcal{N} = \left( \frac{2NL}{c^{N-1}(N-1)!} \right)^{-1/2}. \quad (7)$$

It is computed in detail in appendix A.

## III. THE QUANTUM BRIGHT SOLITON STATE

The aim of this article is to compute the one body density matrix of a quantum bright soliton with a definite number of particles, constructed with Bethe eigenstates.

We want to construct a localized wave packet with massive particles, where quantum superpositions of different particle number are physically not meaningful. It is thus natural to take a superposition of single string states of  $N$  particles with a Gaussian momentum distribution centered on  $P_0 = \frac{\pi}{L} n_0 \in \mathbb{R}$  with width  $\Delta$ . We are considering a box of size  $2L$  with periodic boundary conditions, leading to a discretization of the total momentum of the

strings we are taking in the superposition. The superposed state we are considering is

$$|S\rangle = \mathcal{G} \sum_{n=n_0-\frac{s}{2}}^{n_0+\frac{s}{2}} e^{-\frac{\pi^2}{L^2\Delta}(n-n_0)^2} \left| \frac{N\pi}{L}n \right\rangle, \quad (8)$$

with  $s$  being a threshold we include for our numerical implementation. Ideally, we would like to take it to infinity.  $\mathcal{G}$  is a normalization factor for the discrete Gaussian distribution we are using.

Let us now recall the expression of the one body density matrix in its first quantized form. Given a state  $|S\rangle$  of  $N$  particles, it takes the form

$$\rho(x', x) = N \int_{[-L, L]^{N-1}} dx_1 \dots dx_{N-1} \langle S | x_1, \dots, x_{N-1}, x' \rangle \langle x_1, \dots, x_{N-1}, x | S \rangle. \quad (9)$$

In the case of the state (8), if we define a form factor as

$$\mathcal{F}_{p', p}(x', x) = \int_{[-L, L]^{N-1}} dx_1 \dots dx_{N-1} \langle p' | x_1, \dots, x_{N-1}, x' \rangle \langle x_1, \dots, x_{N-1}, x | p \rangle, \quad (10)$$

we obtain for the density matrix,

$$\rho(x', x) = N \mathcal{G}^2 \sum_{n, n'=n_0-\frac{s}{2}}^{n_0+\frac{s}{2}} e^{-\frac{\pi^2}{L^2\Delta}((n'-n_0)^2 + (n-n_0)^2)} \times \mathcal{F}_{\frac{N\pi}{L}n', \frac{N\pi}{L}n}(x', x). \quad (11)$$

The computation of the form factors requires a numerical implementation. Due to its complexity, it is the aim of the next section to give some details on it.

#### IV. COMPUTATION OF THE FORM FACTOR

In this section we give some details on the computation of the form factors for the density matrix of the solitonic state  $|S\rangle$ .

The expression for the form factor (10) can be simplified by extending the integration domain to  $\mathbb{R}^{N-1}$ , which is justified by the exponential localisation of the expression (8). This assumption leads to an approximation at the same level as neglecting the string deviations in (4). It is valid in the regime  $\frac{1}{c} \ll L$ .

Now, given the symmetry of the integrand, we can rewrite the integral (10) in the fundamental domain to

obtain

$$\begin{aligned} \mathcal{F}_{p', p}(x', x) &= (N-1)! \mathcal{N}^2 \sum_{0 \leq m \leq m' \leq N-1} \int_{-\infty \leq x_1 \leq \dots \leq x_m \leq x \leq x_{m+1} \leq \dots \leq x'_m \leq x' \leq x_{m'+1} \leq \dots \leq x_{N-1} \leq \infty} \{dx_i\} \\ &\exp \left[ i(p x - p' x') + \frac{c}{2}(2m - N + 1)x + \frac{c}{2}(2m' - N + 1)x' \right] \\ &\times \exp \left[ i(p - p') \sum_{j=1}^{N-1} x_j - c \sum_{j=1}^{N-1} (N - 2j)x_j \right] \\ &\times \exp \left[ -c \sum_{j=1}^m x_j + c \sum_{j=m'+1}^{N-1} x_j \right], \quad (12) \end{aligned}$$

with the convention that  $x_0 = -\infty$  and  $x_N = \infty$ .

Trying now to compute one of the integrals of the above sum, we notice that it is the product of three independent factors which are

$$\mathcal{I}_m^1(x', x) = \int_{x_m = -\infty}^x \dots \int_{x_2 = -\infty}^{x_3} \int_{x_1 = -\infty}^{x_2} \{dx_i\} \times e^{i(p-p') \sum_{j=1}^m x_j - c \sum_{j=1}^m (N-2j+1)x_j} \quad (13)$$

$$\mathcal{I}_{m'}^2(x', x) = \int_{x_{m'+1} = x'}^{\infty} \dots \int_{x_{N-2} = x_{N-3}}^{\infty} \int_{x_{N-1} = x_{N-2}}^{\infty} \{dx_i\} \times e^{i(p-p') \sum_{j=m'+1}^{N-1} x_j - c \sum_{j=m'+1}^{N-1} (N-2j-1)x_j} \quad (14)$$

$$\mathcal{I}_{m', m}(x', x) = \int_{x_{m'} = x}^{x'} \dots \int_{x_{m+2} = x}^{x_{m+3}} \int_{x_{m+1} = x}^{x_{m+2}} \{dx_i\} \times e^{i(p-p') \sum_{j=m+1}^{m'} x_j - c \sum_{j=m+1}^{m'} (N-2j)x_j}. \quad (15)$$

It is worth mentioning here that the convergence of these integrals is ensured by the negativity of  $c$ .

The first two factors can be integrated in closed form, and give respectively

$$\begin{aligned} \mathcal{I}_m^1(x', x) &= \frac{1}{m!} \prod_{r=1}^m \frac{1}{-c(N-r) - i(p-p')} e^{im(p-p')x - cm(N-m)x}, \\ &\quad (16) \end{aligned}$$

$$\begin{aligned} \mathcal{I}_{m'}^2(x', x) &= \frac{1}{(N-1-m')!} \prod_{r=1}^{N-1-m'} \frac{1}{c(N-r) - i(p-p')} \\ &\times e^{i(N-1-m')(p-p')x' + c(N-1-m')(m'+1)x'}. \quad (17) \end{aligned}$$

The third factor is more complicated. When we compute one of the successive integrals in  $\mathcal{I}$ , we obtain two terms, corresponding to the upper and lower limit of the integration domain. In the case of the first two factors  $\mathcal{I}^1$

and  $\mathcal{I}^2$ , one of these terms vanishes because of the limit being infinity, but for  $\mathcal{I}$ , none of these terms cancels, and they accumulate in the next integrals.

As a consequence, we recover  $2^{m'-m}$  terms to compute. A numerical implementation is necessary in order to evaluate them. These computations are based on a diagrammatic representation of the integrals, which leads to a reduction of the computational time. The diagrams help sorting out the different terms, in order to factor out their position dependence in certain cases, decreasing the computational time. They are also the basis of the numerical implementation itself.

The diagrammatic representation, the key of the problem, are presented in the next section for the case of a form factor between two different eigenstates. The case of identical eigenstates is discussed in the appendix B, as it requires extra care and is more complex.

## V. FORM FACTOR BETWEEN TWO DIFFERENT EIGENSTATES

In this section, we give some details on the computation of the integral (15). Let us first set the following notation that will be also used in appendix B. We define the partial sum  $u(i, j) = c \sum_{k=i}^j (N - 2j)$ , which yields

$$u_{i,j} = \begin{cases} c(N - i - j)(j - i + 1), & \text{if } i \leq j \\ 0, & \text{otherwise.} \end{cases} \quad (18)$$

We also denote by  $P = (p - p')$  the difference of the momenta between the two strings involved in the form factor we are considering.

The derivation of the form factors involves the computation of a sequence of integrals, each on a different variable, starting by integrating  $x_{m+1}$  until  $x_{m'}$ . Each of these integrations gives rise to two terms, one coming from the lower limit of the integral  $x_i = x$ , and the other one from  $x_i = x_{i+1}$ . Unlike the case of Eqs. (13) and (14), none of these terms vanishes.

First, let us consider the simple case of  $m' = m + 2$  in which we must integrate only over two variables. When we perform the first integral, we get

$$\mathcal{I}_{m',m'-1}(x', x) = \int_x^{x'} dx_{m'} \frac{e^{(iP - u_{m',m'})x_{m'}}}{iP - u_{m'-1,m'-1}} \left( e^{(iP - u_{m'-1,m'-1})x_{m'}} - e^{(iP - u_{m'-1,m'-1})x} \right). \quad (19)$$

We have now two integrals to compute, giving us four terms. To obtain one of these terms, we must have first chosen one of the two integrals in (19), and then either the term associated to the  $x'$  limit or to the  $x$  limit in the remaining integral. This succession of choices can be represented as a diagram. For the simple case of Eq. (19), these are presented in Fig. 1, and are associated to the

four terms in the following equation

$$\mathcal{I}_{m',m'-1}(x', x) = \frac{e^{(2iP - u_{m',m'-1})x'}}{2iP - u_{m',m'-1}} - \frac{e^{(2iP - u_{m',m'-1})x}}{2iP - u_{m',m'-1}} - \frac{e^{(iP - u_{m',m'})x'} - e^{(iP - u_{m'-1,m'-1})x}}{iP - u_{m',m'}} + \frac{e^{(2iP - u_{m',m'-1})x}}{iP - u_{m',m'}}. \quad (20)$$

For a more general  $\mathcal{I}$ , this representation consists in a  $2 \times (m' - m)$  grid, where each column is one of the integrals, and the upper and lower rows represent the upper and lower limits of each integral. For instance, taking the upper point in column  $i$  for a diagram means that for the integral on  $x_i$ , we choose the term corresponding to the upper limit  $x_i = x_{i+1}$ . Note that the diagrams, unlike the integrals, are read from left to right, the first column on the left corresponding to the first integration.

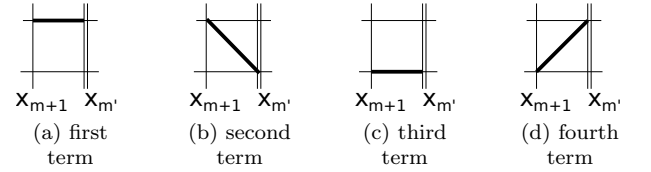


Figure 1: Elementary diagrams, from which more complicated diagrams are constructed. The four diagrams also correspond to the four terms in Eq. (20) from left to right, respectively. Diagram 1a is a 2-diagram, 1b and 1c are 0-diagrams, and 1d is a 1-diagram.

This diagrammatic representation is useful in two ways. From one side, it is a basis for the code that computes these terms, which works constructing recursively all the possible diagrams. From the other side, it also diminishes computational time using the concept of  $l$ -diagrams. We can notice that, given  $m$  and  $m'$ , each term of  $\mathcal{I}_{m',m}$  is of the form

$$\mathcal{C} e^{iP(l'x' + (m' - m - l)x) - u_{m'-l+1,m'}x' - u_{m+1,m'-l}x}, \quad (21)$$

with  $l \in \{0, \dots, (m' - m)\}$ . An  $l$ -diagram is defined as a diagram representing this type of contribution for a given  $l$ . Graphically, it is a diagram that has a number  $l$  of “upper” choices in a row before the last column (last column included), as shown in figures 1 and 2.

To understand the latter form (21) for the exponential dependence and its link to the diagrammatic representation, we must see that when computing an integral associated to a diagram, the result of the  $j$ -th integral (where we integrate over  $x_{m+j}$ ) will depend on the choices we have done for the previous integrals. If, in one of the previous integrals, let's say when we integrate over  $x_i$ , we choose the upper limit term, then its dependence on  $x_{i+1}$  will be carried over to the next integral, while the other choice would lead to a simple prefactor depending

on  $x$ . We can thus notice a very important fact: *whatever the choices for the previous integrals are, as soon as we choose a low term (in the sense of the diagrams), all the choices we have made before this integration will not affect the  $(i+1)$ -th integral and the following integrals.* This is true in particular for the exponential dependence, which is the important part.

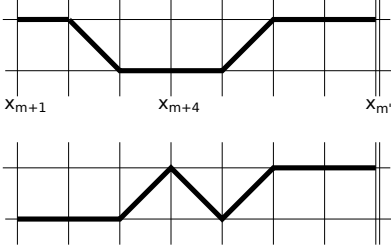


Figure 2: Two examples of 3-diagrams. They both carry the same exponential factor but not the same prefactor. The “fixed” part of the diagrams starts at column 6, while what happens before does not affect the exponential dependence of the whole diagram.

Now, the  $x'$  dependence in Eq. (21) can only come from the last integration, over the variable  $x_{m'}$ . It is thus only determined by the number of “upper choices” in a row starting from the last column of a diagram. The exponential dependence in  $x$  is determined before this succession of upper choices, and thus the final exponential dependence is determined by the number  $l$  of upper choices we make in a row. Two examples of 3-diagrams are presented in Fig. 2.

We can now, instead of computing  $\mathcal{I}$  by summing over all the diagrams, simply sum over the  $l$ -diagrams, i.e. factorize the terms that have the same exponential contribution. For a given  $l$ , we have to compute all the different possible paths until the fixed part starts (see fig 2), because they all carry a different prefactor  $\mathcal{C}$ . This reduces the number of diagrams we have to compute. The huge advantage is that we are interested in computing the density matrix over all the space, and the position dependence only appears in the exponentials. This means that we can store the prefactors, computing them only once for the whole density matrix.

We give here a recursive procedure to compute the prefactor associated to a given diagram. We read the diagrams from left to right, and each step consists in moving forward of one column. Let  $\mathcal{C}_k^n(P, N)$  be the prefactor at step  $n$  for a given difference in momenta  $P$  and a number of particles  $N$  ( $k$  being a memory variable of the number of “upper” terms in a row before the actual step). Then  $\mathcal{C}_{k'}^{n+1}(P, N)$  is obtained by a product

$$\mathcal{C}_{k'}^{n+1}(P, N) = \mathbf{T}_{n+1,k}^i \mathcal{C}_k^n(P, N). \quad (22)$$

The factor  $\mathbf{T}$  and the new memory variable  $k'$  are obtained by identifying which of the four elementary diagram of Fig. 1 lies between the  $(n+1)$ -th and the  $n$ -th

column:

$$\begin{aligned} (1a), (1d): \mathbf{T}_{n,k}^1 &= 1/(iP - u_{n-k,n}), \quad k' = k + 1 \\ (1b), (1c): \mathbf{T}_{n,k}^2 &= -1/(iP - u_{n-k,n}), \quad k' = 0. \end{aligned} \quad (23)$$

We initialize the recursive procedure for the first column  $n_0$  by

$$\mathcal{C}_0^{n_0}(P, N) = \mathbf{T}_{0,0}^i, \quad (24)$$

with  $i = 1$  for a *up* choice and  $i = 0$  for a *low* choice.

The case of identical eigenstates is more complicated, and is explained in detail in appendix B.

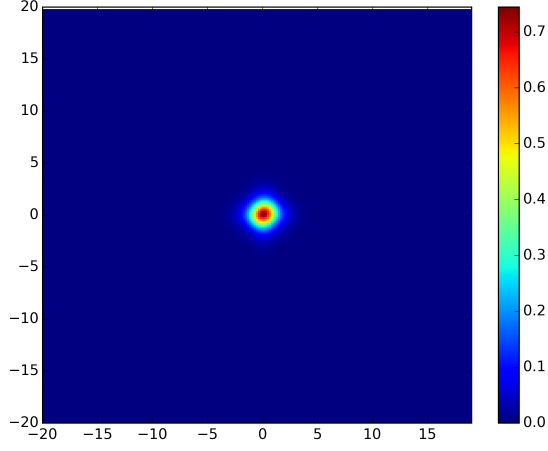
We have thus constructed a method to compute the one body density matrix of our system, which we are going to apply in the next section to give some results.

## VI. RESULTS

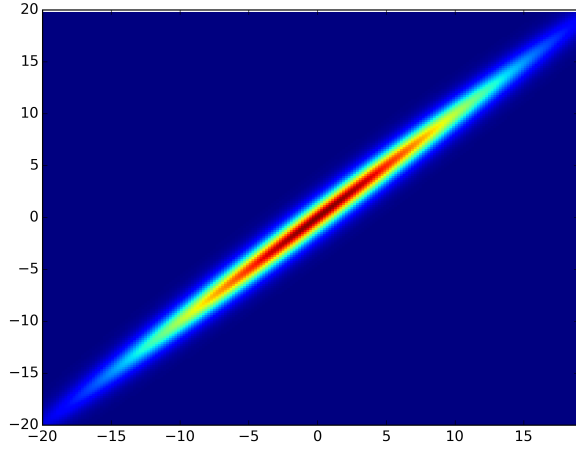
We now show, as an application, some results that are obtained through this method. The free parameters of our code are the number of particles  $N$ , the length of the system  $L$ , the interaction strength  $c$ , the Gaussian width  $\Delta$ , the number of strings we take in our superposed state  $s$ , and the spatial grid width  $\delta x$ . In the following,  $n_0$  is taken equal to zero. The main quantities we are interested in from the density matrix are its eigenvalues, which give the condensed fraction(s) of the state we are studying.

We can first look at the qualitative shape of the density matrix. As we can see from Fig. 3, the density matrix is localized close to the diagonal. For a completely condensed state (i.e. when all the eigenvalues of  $\rho$  are 0 except one), we expect the density matrix to have the four-fold symmetry of a product function, centered on zero. Indeed, in this case, for a solitonic state, the matrix is of the form  $\rho = |G\rangle\langle G|$ , with  $|G\rangle$  being a state with a bell-shaped profile in position representation. The rounder and more elongated the matrix looks like, the more fragmented the condensate is, which means that other eigenstates beyond the dominant one become relevant. When we increase the number of particles keeping the other parameters fixed, we get a state that is more fragmented. Reversely, increasing the number of strings that we take in our superposition increases the condensation. Since  $s$  should be as close to infinity as possible, it should be taken large enough to observe a saturation of the condensed fraction.

Another problem comes from the threshold  $s$ . When we increase  $\Delta$ , we can reach a regime where the soliton is not localized anymore, and we see other peaks in the density appearing on the diagonal. What happens is that the state does not behave like a wave packet anymore: we are willing to take into account too many frequencies with the Gaussian distribution compared to the ones that are really taken in the sum due to the threshold. So in order



(a)  $N = 6$ ,  $c = -0.5$ ,  $s = 7$  and  $\Delta = 0.05$



(b)  $N = 10$ ,  $c = -0.5$ ,  $s = 70$  and  $\Delta = 20$

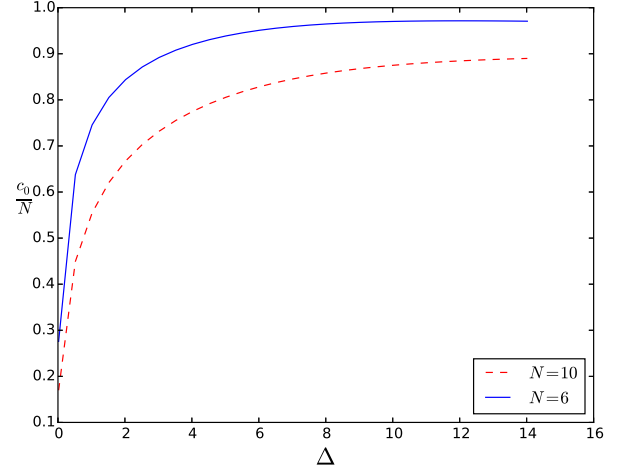
Figure 3: Carpet plot of the one-body density matrix (11) of a soliton state. We can see that 3b is more localized than 3a, meaning a higher condensed fraction.

to be able to scan a wide range of parameter  $\Delta$ , we need to increase  $s$ .

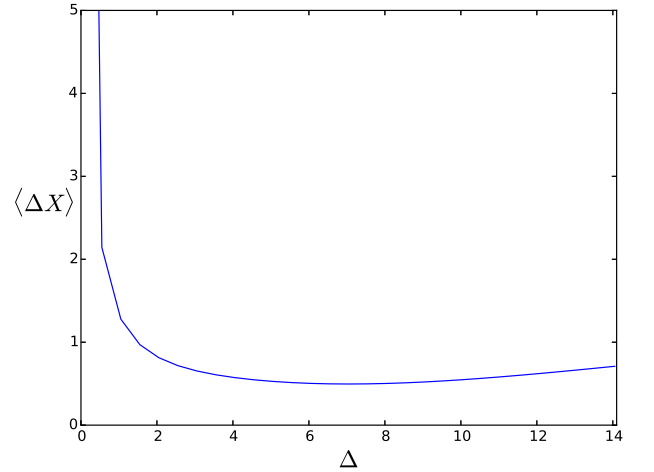
The typical computational time on the NZIAS computer cluster (single CPU, Python implementation) to obtain a density matrix for  $s = 10$  is of 2 hours, and it scales as  $\Theta(s^2)$ .

Interesting quantities are plotted in Fig. 4. It is the variation of the condensed fraction of the soliton and its spreading in space when  $\Delta$  varies. The existence of a minima in the condensed fraction is a very promising result since it shows that there exist an optimal state that we would expect to be linked to the mean field theory soliton. In Fig. 4a we look at the condensed fraction, and see that it saturates to a maximal value of 0.96.

This results are optimized in terms of number of strings,



(a) Maximal eigenvalue of the density matrix versus the width of the state in momentum for different number of particles



(b) Spatial variance  $\langle \Delta X \rangle = \int x^2 \rho(x, x) dx - (\int x \rho(x, x) dx)^2$  of the density matrix along the diagonal versus the width of the state in momentum for  $N = 6$ . Minima of 0.50

Figure 4: Plots of different quantities associate to the density matrix of the solitonic state, for  $s = 70$ ,  $L = 25$ ,  $c = -0.5$  and  $\delta x = 0.3$ . The free parameter is the width of the Gaussian in momentum space  $\Delta$ . We observe that when we increase the width in momentum, we reach a minima of spatial width. We can also see that the condensed fraction  $c_0$  increases more slowly if we take a larger number of strings.

as we can see in Fig. 5 where we have plotted the maximal condensed fraction for different number of strings. At each step, we increase  $\Delta$  until we reach the saturation of the condensed fraction, and then we increase the number of strings.

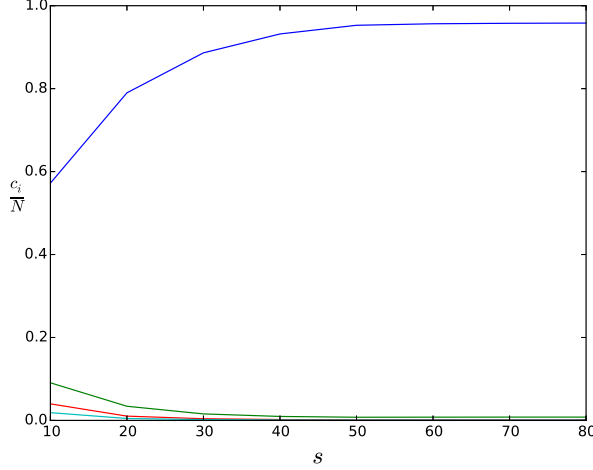


Figure 5: Plot of the four largest eigenvalues of the one-body density matrix of the quantum soliton vs. the string number  $s$ , in the saturation regime of Fig. 4. The parameters are  $L = 20$ ,  $N = 6$ ,  $\delta x = 0.2$  and  $c = -0.5$ .

We are able to reach a condensed fraction of 0.96.

## CONCLUSION

In this article we have presented a method to compute the full one-body density matrix of a quantum bright soliton, based on a numerical evaluation of a diagrammatic formalism.

As an application, we have computed a few relevant quantities, in particular the largest obtainable condensate fraction of a quantum bright soliton with  $N = 6$  particles, with is 96%. The interesting features these results reveal are a motivation for further work aiming to characterize more precisely the optimal state found in terms of spatial variance. Future work will also include the study of time dependence, which can be obtained straightforwardly with the presented approach.

## Appendix A: Norm of the Lieb-Liniger eigenstates

In this appendix, we prove Eq. (7). This norm is the one used for our numerical calculations. We want the eigenstates of the system to be normalized to one, and the trace of the density function to be  $N$ . When we compute the density function (9), we discretise space on a grid of spacing  $\delta x$ . This means that the actual condition for the normalization of the density function is

$$\delta x \sum_{k=-L/\delta x}^{L/\delta x} \rho(k \delta x, k \delta x) = N. \quad (\text{A1})$$

We can infer from this that, when computing the norm of the eigenstates, we are going to discretise only the last variable  $x_N$ , which is the only one that is not integrated

in the definition of the density function, and on which we sum over in (A1).

The condition for the normalization of the eigenstates is thus

$$\begin{aligned} \langle p|p \rangle &= \mathcal{N}^2 \sum_{k=-L/\delta x}^{L/\delta x} \delta x \int_{[-L, L]^{N-1}} dx_1 \dots dx_{N-1} \\ \langle p|x_1, \dots, x_{N-1}, k \delta x \rangle \langle x_1, \dots, x_{N-1}, k \delta x|p \rangle &= 1. \end{aligned} \quad (\text{A2})$$

As in Sec. IV, we can first extend the integration domain to  $[-\infty, \infty]^{N-1}$ , and also, given the symmetry of the integrand, rewrite it in the fundamental domain  $-\infty \leq x_1 \leq \dots \leq x_{N-1} \leq i \delta x \leq \infty$ . We thus obtain

$$\begin{aligned} \mathcal{N}^{-2} &= N! \delta x \sum_{k=-L/\delta x}^{L/\delta x} \int_{-\infty}^{k \delta x} dx_{N-1} \dots \int_{-\infty}^{x_2} dx_1 \\ &\quad \times e^{c \sum (N-2j+1)x_j + c k \delta x} \\ &= N! \delta x \sum_{k=-L/\delta x}^{L/\delta x} \frac{1}{c(N-j)j} \prod_{j=1}^{N-1} \frac{1}{c(N-j)j} \\ &= \frac{N! \delta x}{c^{N-1} (N-1)!^2} \frac{2L}{\delta x}. \end{aligned} \quad (\text{A3})$$

Thus we recover Eq. (7).

## Appendix B: Form factor involving identical eigenstates

In Section V, we explained how we can construct a diagrammatic representation that simplifies the computation of the integral  $\mathcal{I}$  in the case of  $P \neq 0$ . Here we consider the case of  $P = 0$ . This case occurs when the argument of the exponential we are integrating is real, and is of the form  $-u_{i,j}$  (see Eq. (18) for the definition), and can vanish. It is the case when  $j + i = N$ . A very important fact to notice is that *it can only vanish once per diagram*. If the argument of the exponential is different from zero, we can use the same representation as in Section V.

Let's assume that the cancellation happens for the integral on the variable  $x_{n-1}$ . Then the result of this integration will be  $(x_n - x)$ . When we compute the integral over  $x_{n+1}$ , we obtain

$$\int_x^{x_{n+1}} dx_n x_n e^{-u_{n,n} x_n} - x \int_x^{x_{n+1}} dx_n e^{-u_{n,n} x_n}. \quad (\text{B1})$$

The second term follows the usual scheme of appendix V, but the first term requires an integration by parts. After performing it, we get

$$\frac{x_{n+1}}{u_{n,n}} e^{-u_{n,n} x_{n+1}} - \frac{1}{u_{n,n}^2} e^{-u_{n,n} x} + \frac{1 - u_{n,n} x}{u_{n,n}^2} e^{-u_{n,n} x}. \quad (\text{B2})$$

Equation (B2) contains three different types of terms, the first one will induce a new integration by parts in the next integral, the second one will act as a common *up* choice in the diagram, and the third one as a *low* choice (this is inferred from the exponential dependence it is carrying). What happens in this case is that the diagram faces a bifurcation: after the cancellation of the argument of the exponential, a new line of choices is added, as shown in Fig. 6. A consequence of the fact that  $u$  can only vanish once per diagram is that we will only have one bifurcation per diagram, so we will never reach the case where we would have a double integral by parts to perform (with an integrand of the type  $x^2 e^{ux} dx$ ).

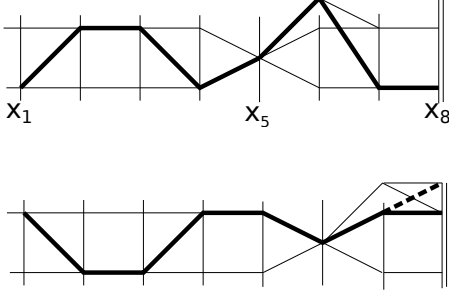


Figure 6: Examples of bifurcations for the case  $N = 10$ .

In the upper case, the cancellation of the exponential argument occurs when integrating  $x_5$  (it is  $u_{5,5}$ ) and in the second case for  $x_6$  ( $u_{4,6}$ ). These are the bifurcation points, where we have then three choices. The upper row cannot be reached by one of the lower rows, as it is the row where integrations by part are performed ( $\alpha = 1$ ). The dashed line represents an example of a diagram that would not be allowed.

In the case where we are computing a form factor involving identical eigenstates, we have to change the recursion relation of Section V adding a new memory variable  $\alpha \in \{0, 1\}$  that stores the fact that an integration by parts is occurring. When constructing or reading the diagrams, we have two different regimes. The case where  $\alpha = 0$  is computed in the exact same way than previously, using relations (23). The regime  $\alpha = 1$  is different and needs new relations. We give now the formula allowing to compute the contribution associated to a given diagram

$$\mathcal{C}_{k', \alpha'}^{n+1}(P, N) = \mathbf{Q}_{n+1, k, \alpha}^i \mathcal{C}_{k, \alpha}^n(P, N). \quad (\text{B3})$$

The rules for the transition factor  $\mathbf{Q}$  are associated to the elementary diagrams of Figs. 1 and 7. We give here these relations, and the couple of new memory variables

$(k', \alpha')$ :

$$\begin{aligned} (1a), (1d): \mathbf{Q}_{n, k, 0}^1 &= 1 / (-u_{n-k, n}), (k+1, \alpha), \\ (1b), (1c): \mathbf{Q}_{n, k, 0}^2 &= -1 / (-u_{n-k, n}), (0, 0), \\ (7a): \mathbf{Q}_{n, k, 0}^3 &= 1, (0, 1), \text{ only for } (2n-k) = N, \\ (7b): \mathbf{Q}_{n, k, 1}^1 &= 1 / (-u_{n-k, n}), (\{0, k+1\}, \{0, 1\}), \\ (7c): \mathbf{Q}_{n, k, 1}^2 &= 1 / (u_{n-k, n}^2), (\{0, k+1\}, 0), \\ (7d): \mathbf{Q}_{n, k, 1}^3 &= (u_{n-k, n} x - 1) / (u_{n-k, n}^2), (0, 0). \end{aligned} \quad (\text{B4})$$

In the above relations, it is important to add that  $\mathbf{Q}_{n, k, 0}^3$  can be used, and must be used only when the cancellation in the exponential occurs, which is the condition explicated in (B4), equivalent to  $u_{n-k, n} = 0$ .

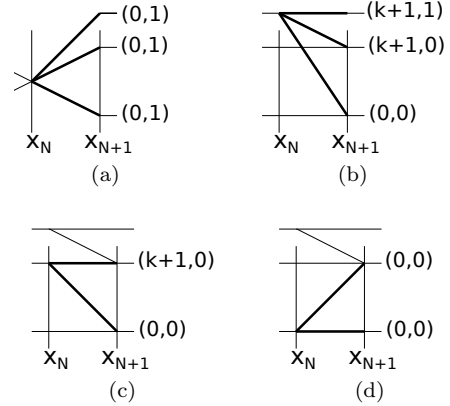


Figure 7: Additional elementary diagrams for the case of a form factor between the same eigenstates. The diagram 7a is the bifurcation diagram, and the three other diagrams are the elementary diagrams in the regime  $\alpha = 1$ . Bold lines represent the different possibilities in each case, associated with the couple  $(k', \alpha')$  of new memory variables. When  $\alpha = 0$ , refer to Fig. 1.

As a final remark, we highlight that the complexity of this case is increased due to the fact that even the grid on which the diagrams are drawn can change according to the previous choices, between the regime  $\alpha = 1$  where it is a three-row grid and the  $\alpha = 0$  case where it has only two rows. The moment in which the bifurcation occurs depends on the previous choices of diagrams, but it can only occur once for a given diagram.

## REFERENCES

- <sup>1</sup>M. A. Cazalilla, R. Citro, T. Giamarchi, E. Orignac, and M. Rigol, “One dimensional bosons: From condensed matter systems to ultracold gases,” *Rev. Mod. Phys.* **83**, 1405–1466 (2011).
- <sup>2</sup>Y.-Z. Jiang, Y.-Y. Chen, and X.-W. Guan, “Understanding many-body physics in one dimension from the Lieb–Liniger model,” *Chinese Phys. B* **24**, 050311 (2015).
- <sup>3</sup>N. Fabbri, M. Panfil, D. Clément, L. Fallani, M. Inguscio, C. Fort, and J.-S. Caux, “Dynamical structure factor of one-dimensional



- Bose gases: Experimental signatures of beyond-Luttinger-liquid physics,” *Phys. Rev. A* **91**, 043617 (2015), arXiv:1406.2176.
- <sup>4</sup>J. Armijo, T. Jacqmin, K. V. Kheruntsyan, and I. Bouchoule, “Probing three-body correlations in a quantum gas using the measurement of the third moment of density fluctuations,” *Phys. Rev. Lett.* **105**, 3–6 (2010), arXiv:1007.3713.
- <sup>5</sup>B. Paredes, A. Widera, V. Murg, O. Mandel, S. Foelling, I. Cirac, G. V. Shlyapnikov, T. W. Hansch, and I. Bloch, “Tonks-Girardeau gas of ultracold atoms in an optical lattice,” *Nature* **429**, 277–281 (2004).
- <sup>6</sup>T. Kinoshita, T. Wenger, and D. S. Weiss, “Observation of a One-Dimensional Tonks-Girardeau Gas,” *Science* (80-. ). **305**, 1125 (2004).
- <sup>7</sup>E. Lieb and W. Liniger, “Exact analysis of an interacting Bose gas. I. The general solution and the ground state,” *Phys. Rev.* , 1605–1616 (1963); E. H. Lieb, “Exact analysis of an interacting Bose gas. II. the excitation spectrum,” *Phys. Rev.* **130**, 1616–1624 (1963).
- <sup>8</sup>B. Sutherland, *Beautiful Models: 70 Years of Exactly Solved Quantum Many-body Problems* (World Scientific, Singapore, 2004) p. 381.
- <sup>9</sup>V. Korepin, N. Bogoliubov, and A. Izergin, *Quantum Inverse Scattering method and correlation functions* (Cambridge monographs on mathematical physics).
- <sup>10</sup>V. E. Korepin, “Calculation of norms of Bethe wave functions,” *Commun. Math. Phys.* **86**, 391–418 (1982).
- <sup>11</sup>P. Calabrese and J.-S. Caux, “Dynamics of the attractive 1D Bose gas: analytical treatment from integrability,” *J. Stat. Mech. Theory Exp.* , 08032–08032 (2007).
- <sup>12</sup>F. Calogero and A. Degasperis, “Comparison between the exact and Hartree solutions of a one-dimensional many-body problem,” *Phys. Rev. A* **11**, 265–269 (1975).
- <sup>13</sup>Y. Castin, “Internal structure of a quantum soliton and classical excitations due to trap opening,” *Eur. Phys. J. B* **68**, 317–328 (2008).
- <sup>14</sup>Y. Lai and H. A. Haus, “Quantum theory of solitons in optical fibers. ii. exact solution,” *Phys. Rev. A* **40**, 854–866 (1989).
- <sup>15</sup>J. C. Zill, T. M. Wright, K. V. Kheruntsyan, T. Gasenzer, and M. J. Davis, “A coordinate Bethe ansatz approach to the calculation of equilibrium and nonequilibrium correlations of the one-dimensional Bose gas,” 1601.00434 (2016), arXiv:1601.00434.
- <sup>16</sup>J. H. V. Nguyen, P. Dyke, D. Luo, B. a. Malomed, and R. G. Hulet, “Collisions of matter-wave solitons,” *Nat. Phys.* **10**, 1–5 (2014).
- <sup>17</sup>P. Medley, M. A. Minar, N. C. Cizek, D. Berryrieser, and M. A. Kasevich, “Evaporative production of bright atomic solitons,” *Phys. Rev. Lett.* **112**, 1–5 (2014).
- <sup>18</sup>A. L. Marchant, T. P. Billam, T. P. Wiles, M. M. H. Yu, S. A. Gardiner, and S. L. Cornish, “Controlled formation and reflection of a bright solitary matter-wave,” *Nat. Commun.* **4**, 1865 (2013), arXiv:1301.5759.
- <sup>19</sup>S. L. Cornish, S. T. Thompson, and C. E. Wieman, “Formation of bright matter-wave solitons during the collapse of attractive Bose-Einstein condensates,” *Phys. Rev. Lett.* **96**, 1–4 (2006), arXiv:0601664 [cond-mat].
- <sup>20</sup>L. Khaykovich, F. Schreck, G. Ferrari, T. Bourdel, J. Cubizolles, L. Carr, Y. Castin, and C. Salomon, “Formation of a matter-wave bright soliton,” *Science* (80-. ). **296**, 1290–1294 (2002).
- <sup>21</sup>C. Weiss and Y. Castin, “Creation and detection of a mesoscopic gas in a nonlocal quantum superposition,” *Phys. Rev. Lett.* **102**, 010403 (2009).
- <sup>22</sup>R. Kanamoto, H. Saito, and M. Ueda, “Symmetry breaking and enhanced condensate fraction in a matter-wave bright soliton,” *Phys. Rev. Lett.* **94**, 090404 (2005).
- <sup>23</sup>Y. Lai and R.-K. Lee, “Entangled quantum nonlinear Schrödinger solitons,” *Phys. Rev. Lett.* **103**, 013902 (2009).
- <sup>24</sup>J. B. McGuire, “Study of exactly soluble one-dimensional n-body problems,” *J. Math. Phys.* **5**, 622 (1964).
- <sup>25</sup>V. Zakharov and A. Shabat, “Exact theory of two-dimensional self-focusing and one-dimensional self-modulation of waves in nonlinear media,” *Sov. Phys. JETP* **34**, 62–65 (1972).